JACS ARTICLES

Published on Web 07/29/2010

The Development of Morphology and Structure in Hexagonal Vaterite

Emilie M. Pouget, Paul H. H. Bomans, Archan Dey, Peter M. Frederik, Gijsbertus de With, and Nico A. J. M. Sommerdijk*

Laboratory of Materials and Interface Chemistry and Soft Matter CryoTEM Research Unit, Eindhoven University of Technology, P.O. Box 513, 5600MB Eindhoven, The Netherlands

Received April 3, 2010; Revised Manuscript Received July 12, 2010; E-mail: N.Sommerdijk@tue.nl

Abstract: Inspired by the remarkable shapes and properties of $CaCO_3$ biominerals, many studies have investigated biomimetic routes aiming at synthetic equivalents with similar morphological and structural complexity. Control over the morphology of $CaCO_3$ crystals has been demonstrated, among other methods, by the use of additives that selectively allow the development of specific crystal faces, while inhibiting others. Both for biogenic and biomimetic $CaCO_3$, the crystalline state is often preceded by an amorphous precursor phase, but still limited information is available on the details of the amorphous-to-crystalline transition. By using a combination of cryoTEM techniques (bright field imaging, cryo-tomography, low dose electron diffraction and cryo-darkfield imaging), we show for the first time the details of this transition during the formation of hexagonal vaterite crystals grown in the presence of NH_4^+ ions. The formation of hexagonal plate-like vaterite occurs via an amorphous precursor phase. This amorphous phase converts into the crystalline state through a solid state transformation in which order and morphology develop simultaneously. The mineral initially develops as polycrystalline vaterite which transforms into a single crystal directed by an NH_4^+-induced crystal plane that acts as a templating surface.

Introduction

Inspired by the remarkable shapes and properties of $CaCO_3$ biominerals, many studies have investigated biomimetic routes aiming at synthetic equivalents with similar morphological and structural complexity.[1,2] For several $CaCO_3$ biominerals, it was shown that they grow within a dedicated compartment in which biomacromolecules control the shape and the polymorphic type of the mineral, as well as its crystallographic habit.[3] In a laboratory environment, control over the morphology of $CaCO_3$ crystals has been demonstrated by confining growth of the mineral to a preshaped compartment, but also by the use of additives that selectively allow the development of specific crystal faces, while inhibiting others.[1,2,4] In many cases, the latter approach also leads to the destabilization of the thermodynamically preferred polymorph, calcite, in favor of the normally less stable phases, vaterite and aragonite. For example, in the presence of NH_4^+ ions or NH_3^+-bearing additives, vaterite platelets with an unusual hexagonal morphology can be obtained.[5−8] The ammonium groups of the additives stabilize the normally unfavorable (00.1) plane of vaterite, the expression of which gives rise to hexagonal tablet-like crystals.

It has been shown, both for biogenic[9−11] and biomimetic $CaCO_3$,[12−17] that the formation of the crystalline state is often preceded by an amorphous precursor phase. Still, limited information is available on the details of the amorphous-to-crystalline transition, and both solid state transformations[12,13] as well as dissolution-reprecipitation mechanisms[14] have been proposed. Even less information is available on how the development of structure coincides with the development of the crystal morphology and the expression of the stabilized crystal faces.

We recently demonstrated the combination of cryoTEM, low dose selected area electron diffraction (LDSAED), and cryo-electron tomography (cET) as a powerful approach to study the development of crystallinity in template-directed $CaCO_3$ forma-

(1) Sommerdijk, N. A. J. M.; de With, G. *Chem. Rev.* **2008**, *108*, 4499–4550.
(2) Cölfen, H.; Meldrum, F. C. *Chem. Rev.* **2008**, *108*, 4332–4432.
(3) See e.g., (a) Addadi, L.; Joester, D.; Nudelman, F.; Weiner, S. *Chem.—Eur. J.* **2006**, *12*, 980–987. (b) Young, J. R.; Davis, S. A.; Bown, P. R.; Mann, S. *J. Struct. Biol.* **1999**, *126*, 195–215.
(4) Gower, L. B. *Chem. Rev.* **2008**, *108*, 4551–4627.
(5) Xu, A.-W.; Antonietti, M.; Cölfen, H.; Fang, Y.-P. *Adv. Funct. Mater.* **2006**, *16*, 903–908.
(6) Gehrke, N.; Cölfen, H.; Pinna, N.; Antonietti, M.; Nassif, N. *Cryst. Growth Des.* **2005**, *5*, 1317–1319.
(7) Huang, J. H.; Mao, Z. F.; Luo, M. F. *Mater. Res. Bull.* **2007**, *42*, 2184–2191.
(8) Dupont, L.; Portemer, F.; Figlarz, M. *J. Mater. Chem.* **1997**, *7*, 797–800.
(9) Addadi, L.; Raz, S.; Weiner, S. *Adv. Mater.* **2003**, *15*, 959–970.
(10) Politi, Y.; Metzler, R. A.; Abrecht, M.; Gilbert, B.; Wilt, F. H.; Sagi, I.; Addadi, L.; Weiner, S.; Gilbert, P. U. P. A. *Proc. Natl. Acad. Sci. U.S.A.* **2008**, *105*, 17362–17366.
(11) Politi, Y.; Arad, T.; Klein, E.; Weiner, S.; Addadi, L. *Science* **2004**, *306*, 1161–1164.
(12) Pouget, E. M.; Bomans, P. H. H.; Goos, J. A. C. M.; Frederik, P. M.; de With, G.; Sommerdijk, N. A. J. M. *Science* **2009**, *323*, 1455–1458.
(13) Pichon, B. P.; Bomans, P. H. H.; Frederik, P. M.; Sommerdijk, N. A. J. M. *J. Am. Chem. Soc.* **2008**, *130*, 4034–4040.
(14) Lee, J. R. I.; Willey, T. M.; Han, Y.; van Buuren, T.; De Yoreo, J. J. *J. Am. Chem. Soc.* **2007**, *129*, 10370–10381.
(15) Han, T. Y. J.; Aizenberg, J. *Chem. Mater.* **2008**, *20* (3), 1064–1068.
(16) Aizenberg, J.; Muller, D. A.; Grazul, J. L.; Hamann, D. R. *Science* **2003**, *299*, 1205–1208.
(17) Gower, L. B.; Odom, D. J. *J. Cryst. Growth* **2000**, *210*, 719–734.

10.1021/ja102439r

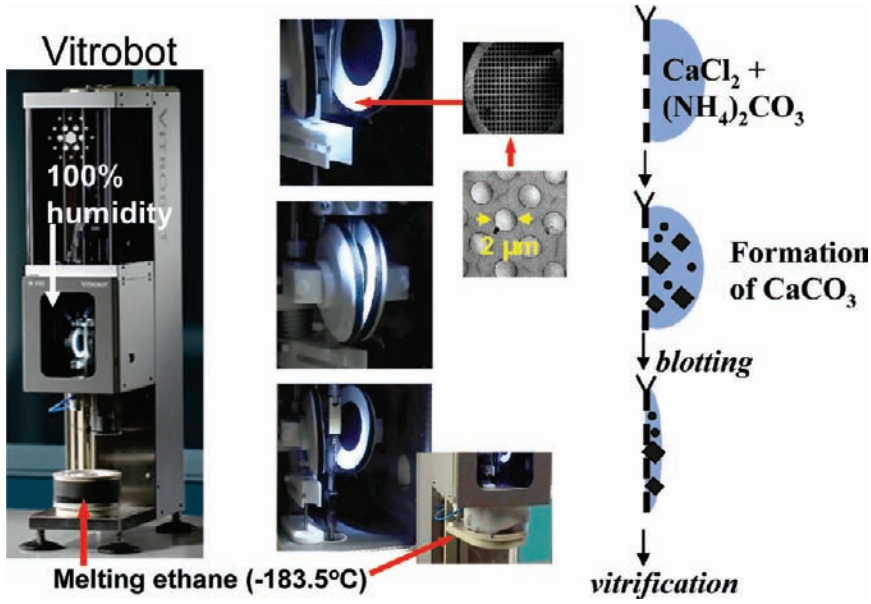

Figure 1. (Left) The Vitrobot Mark III. The temperature and humidity are controlled to be 22 °C and 100% relative humidity. (Center) Visualization of the blotting inside the Vitrobot chamber showing the grid with holey carbon support film held in a pair of tweezers between the blotting pads (top), the removal of the excess liquid by automated blotting (middle), and the plunging of the sample in melting ethane (bottom). (Right) Schematic representation of the sample preparation showing the deposition of the solutions (top) and mineral formation (middle) on the grid followed by the blotting (bottom) and subsequent fixation of the reaction mixture through plunge freeze vitrification.

tion.[12] In the present paper, we use these techniques (cryoTEM, LDSAED, and cET) in combination with dark field imaging to show for the first time, and in detail, the simultaneous development of structure and the expression of crystal planes for hexagonal vaterite crystals grown in the presence of NH_4^+ ions.

Results and Discussion

$CaCO_3$ was synthesized in presence of the NH_4^+ ions by mixing solutions containing 10 mM $CaCl_2$ and 10 mM $(NH_4)_2CO_3$, respectively. The resulting mixture was immediately applied onto a transmission electron microscopy (TEM) grid coated with a perforated carbon film, inside the chamber of an automated vitrification robot (FEI Vitrobot Mark III), which had been set to 22 °C and 100% relative humidity (Figure 1 and Supporting Information 1).[18] Using this procedure, the development of $CaCO_3$ occurs within the solution on the grid and can be arrested at any given time point by vitrification through plunging in melting ethane. After removing the excess of liquid by automated blotting, thin aqueous films were vitrified at different reaction times between 5 and 60 min and investigated using cryoTEM. The pH of the solution was measured to be 8.7 and stable during the course of the reaction.

In accordance with the literature,[5−8] the $CaCO_3$ crystals formed in presence of NH_4^+ ions displayed a hexagonal platelike morphology. Mature hexagonal crystals were obtained after a reaction time of 60 min (Figure 2). The electron diffraction patterns of crystals lying on their large hexagonal faces identified them as vaterite with the zone axis of the exposed face being [00.1]. The stabilization of the nonequilibrium (00.1) face of vaterite has been attributed to the presence of the NH_4^+ ions interacting with the carbonate ions present in this charged crystal plane.[5−8]

(18) Vos, M. R.; Bomans, P. H. H.; Frederik, P. M.; Sommerdijk, N. A. J. M. *Ultramicroscopy* **2008**, *108*, 1478–1483.

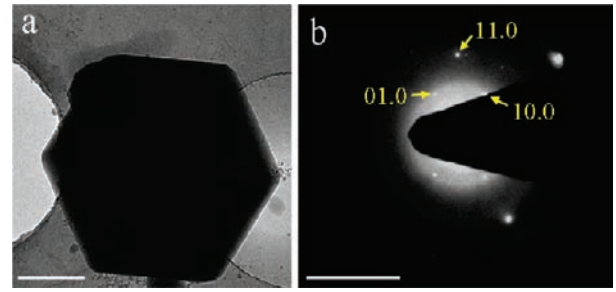

Figure 2. (a) CryoTEM image of a hexagonal vaterite platelet obtained after a time reaction of 60 min. Scale bar = 300 nm. (b) LDSAED pattern of the crystal revealing the [00.1] zone axis of vaterite. Scale bar = 5 nm^{-1}.

To unravel the formation mechanism of these hexagonal platelike crystals, we isolated and studied different stages of the reaction by using a combination of cryoTEM techniques. In the early stages of the reaction (5−10 min), the mineral was present in the form of small amorphous calcium carbonate (ACC) nanoparticles. Size analysis of about 130 particles showed a bimodal size distribution over two populations. One population had a diameter of approximately 35 nm, while the other population had a predominant size of around 70 nm (Figure 3). This bimodal size distribution suggests that the two populations of ACC particles have different stabilities. Recently, we observed a similar bimodal distribution of ACC particles with diameters of ∼30 and 70−100 nm, respectively, when growing calcium carbonate from a supersaturated calcium bicarbonate solution in the presence of a Langmuir monolayer. In these experiments, the ∼30 nm ACC nanoparticles were observed in solution, while the larger population was exclusively observed in conjunction with the monolayer template.[12] The existence of a narrow size distribution of nanoparticles in solution was attributed to an optimal surface area/volume ratio for the relatively unstable amorphous phase. The observation of a second, larger population was attributed to the effect of the

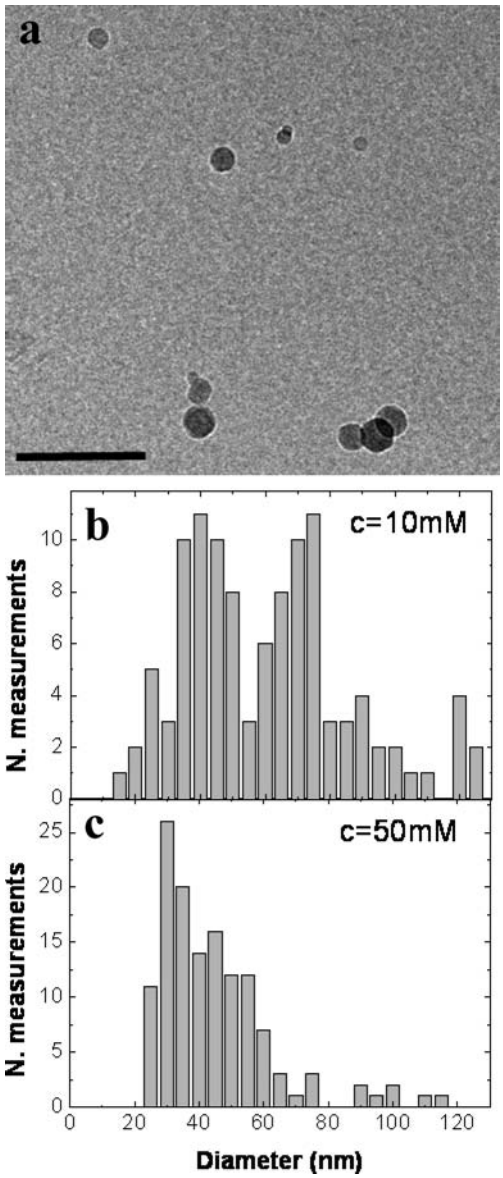

Figure 3. The early stages: (a) cryoTEM image of ACC particles. Scale bar = 200 nm. (b) Size distribution of the ACC particles for the concentration $c = 10$ mM. $N = 130$. (c) Size distribution of the ACC particles for the concentration $c = 50$ mM. $N = 132$.

monolayer, stabilizing the particles and allowing them to grow out beyond the optimal diameter in solution and to develop a new optimal size of 70−100 nm at the air−water interface.

However, in the present case, both populations are formed in the presence of the additive (i.e., the ammonium ions) which is homogeneously present throughout the solution. We must therefore assume that here the formation of a second population of larger and hence more stable ACC particles is due to the kinetics of the reaction rather than to the presence of ammonium ions. Indeed, when we changed the reaction kinetics by performing the reaction with 50 mM $CaCl_2$ and $(NH_4)_2CO_3$ solutions, the analysis of a similar population ($N = 132$) revealed a single broad distribution of ACC nanoparticles with diameters between 25 and 70 nm. We speculate that the two populations formed from the 10 mM solutions may consist of two forms ACC with different degrees of structural order and/or different degrees of hydration.[9,13,23]

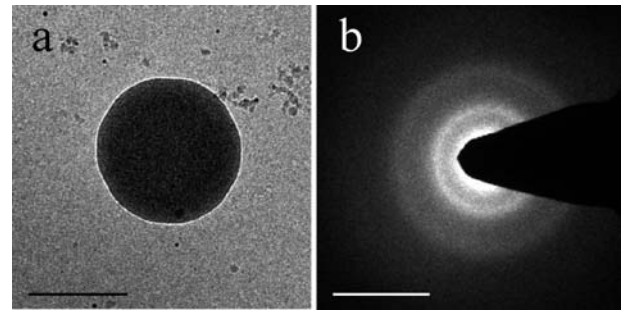

Figure 4. (a) CryoTEM image showing shapeless $CaCO_3$ particle formed after 20 min. Scale bar = 200 nm. (b) The corresponding LDSAED pattern showing its amorphous nature. Scale bar = 5 nm^{-1}.

In the following stage (10−20 min), we observed particles of 200−600 nm that did not display any specific shape in 2D cryoTEM (Figure 4a). LDSAED patterns recorded from these particles showed that some of them displayed broad rings typical for ACC (Figure 4b). In other cases, particles with similar shapes produced electron diffraction patterns in which these broad amorphous bands were overlaid with spot patterns (Figure 5). The latter observation points to a situation in which crystalline domains have developed within an amorphous matrix. For the particle displayed in Figure 5, the two characteristic amorphous rings (Figure 5b, red arrows) could be assigned to ACC.[12] The superimposed diffraction pattern shows diffraction spots corresponding to the *d*-spacings of vaterite, but no indexation was possible, indicating the presence of domains with different crystallographic orientations. The LDSAED patterns of the three highlighted domains of the particle (Figure 5a, yellow circles 1, 2, and 3) confirm the presence of different crystalline areas. Area **1** corresponds to a well-defined crystalline domain of vaterite with the $(1\bar{2}.2)$ plane oriented to the electron beam (Figure 5, **1**). In contrast, the diffraction patterns of area **2** and **3** show spots corresponding to the *d*-spacings of vaterite, but no specific orientations could be assigned implying that also in this smaller zone different crystalline domains are coexisting. The dark field images (Figure 5, **2** and **3**, insets) corresponding to the marked spots (yellow circles) confirmed that these diffraction patterns relate to different crystalline domains. Hence, this $CaCO_3$ particle contains different crystalline domains distributed inside an ACC matrix. These observations are in line with our previous studies of the development of crystallinity in template stabilized calcium carbonate particles[12] as well as with the model system of Zhang et al.[19] In both cases, the development of multiple crystalline domains was indicated inside an amorphous matrix prior to the formation of a single crystal.

However, the presence of crystalline domains prompted us to a more detailed inspection of the morphology of these particles by imaging under different tilt angles. In Figure 5, it is demonstrated how the apparent shape of a crystal may change under different observation angles (tilt-series in Supporting Information 2). However, for a complete 3D view of the crystals, we preformed cryo-electron tomography (3D cryoTEM). To this end, series of cryoTEM images were recorded under different angles with respect to the electron beam up to 70°, with intervals of 2°. From the resulting tilt-series, the corresponding 3D volumes were reconstructed using the Simultaneous Iterative Reconstruction Technique (SIRT). The reconstructed tomogram

(19) Zhang, T. H.; Liu, X. Y. *J. Am. Chem. Soc.* **2007**, *129*, 13520–1352.

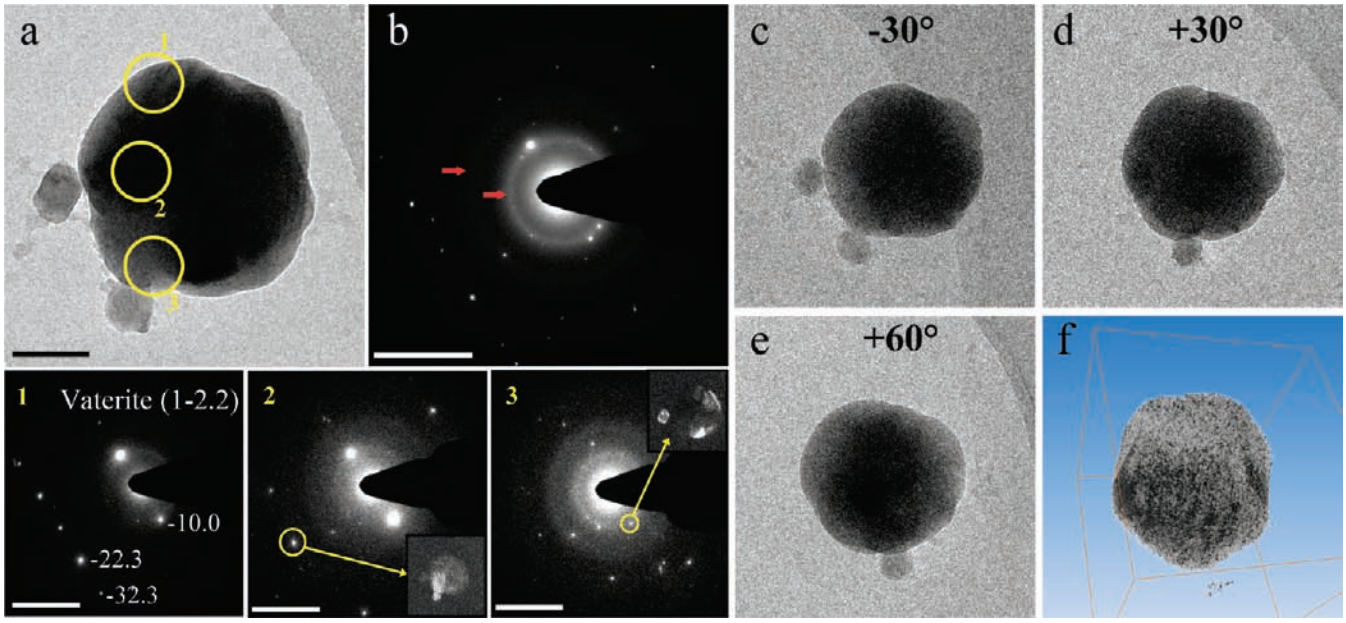

Figure 5. Intermediate stage (20 min reaction). (a) CryoTEM image (scale bar = 200 nm). (b) Electron diffraction pattern of the entire particle in which all the different orientations of the vaterite crystal domains present in the particle appear (scale bar = 5 nm^{-1}). The red arrows indicate the diffuse rings characteristic for ACC.[12] The diffraction patterns 1−3 (bottom) are the LDSAED patterns of the three domains indicated in the cryoTEM image. Pattern 1 corresponds to a well-defined vaterite domain with [1$\bar{2}$.2] orientation. The patterns 2 and 3 represent *d*-spacings corresponding to vaterite but cannot be indexed, due to the polycrystallinity of the domain. The dark field images (insets) generated from the marked spot show different crystalline domains with this same crystallographic orientation. (c−e) CryoTEM images of the particle (a) observed under different angles with respect to the electron beam. (f) 3D reconstruction of the cET showing a poorly developed hexagonal shape. The movies of the cET tilt-series and the 3D reconstruction are presented in Supporting Information 2.

of the apparently shapeless particle in Figure 5 revealed that this polycyrstalline particle indeed already showed the first stadia of facet formation (Figure 5f).

CryoTEM imaging under different tilt angles in combination with LDSAED was also very informative when studying the development of structure and morphology in the later stages of the process. This was demonstrated in the study of particles with varying degrees of morphological development analyzed after reaction times of 20−40 min. In this time interval, mostly irregularly shaped particles (∼200−800 nm) had developed in which different stages of crystallinity could be observed. Interestingly, the evolution of facets observed in the cryoTEM images was not necessarily accompanied by the development of structure, as judged from the acquired diffraction patterns. This is illustrated clearly in Figure 6 where all three particles show the development of facets but display strongly different diffraction patterns. Where particle (a) gives rise only to broad amorphous diffraction rings superimposed onto a polycrystalline spot pattern, the pattern recorded for particles (c) already showed a dominating pattern for the [$\bar{1}\bar{1}$.1] plane. Most surprising, however, was the pattern recorded for the fully developed hexagonal tablet (Figure 6e). Rather than the expected single crystalline pattern, this particle gave rise to broad rings with only very faint spots superimposed on them. This indicates that while the morphology of the particles is already fully developed, the evolution of structure is only just starting.

As the tilting of samples in the electron microscopy setup used was limited to angles between −70 and 70°, some features can only be revealed by full tomographic analysis as exemplified in Figure 7. The diffraction pattern of the particle in this figure showed clearly that it was polycrystalline, and that the amorphous phase is no longer present. Whereas from the tilted images this was not directly visible, cryo-electron tomography showed that despite its polycrystalline nature the particle possessed one fully developed hexagonal (00.1) face (Figure 7c,d and Supporting Information 2). The existence of such a well-defined (00.1) face in a polycrystalline particle implies that this face is formed by domains that all aligned in the (00.1) direction, but with respect to each other are rotated around the crystallographic *c*-axis. This selective stabilization of the (00.1) face can only be explained by the selective interaction of this face with the NH^{4+} ions. Moreover, the observation of the different combinations of structure and morphology displayed in Figures 5 and 6 demonstrates that crystallinity and shape develop separately in these intermediate stages of the formation of the $CaCO_3$ crystals.

Mechanistic Considerations. Vaterite crystallizes in a unit cell that can be described either as orthorhombic[20] or hexagonal.[21] In many cases, vateritic particles do not show very well-defined morphologies and agglomerate to form spherical aggregates.[22] On the basis of symmetry considerations, this hexagonal morphology should expose the (00.1) faces. However, these are high energy faces as they are composed of only CO_3^{2-} or Ca^{2+} ions in an hexagonal orientation.[5] Nevertheless, this unfavorable (00.1) plane of vaterite can be stabilized through the presence of ammonium ions or ammonium bearing additives interacting with the carbonate ions in this crystal plane which gives rise to hexagonal tablet-like crystals. In the present case, the development of this ammonium stabilized (00.1) face is occurring within particles that are still polycrystalline or even partially amorphous.

The first step in the nucleation process is the formation of ∼35 nm ACC nanoparticles. Although we have not demonstrated it in the present paper, we must assume that they form through the aggregation of nanometer sized prenucleation

(20) Wyckoff, R. W. G. *Crystal Struct.* **1964**, *2*, 364.
(21) Meyer, H. J. *Z. Kristallogr.* **1969**, *128*, 183–212.
(22) Davies, P.; Dollimore, D.; Heal, G. R. *J. Therm. Anal.* **1978**, *13*, 473–487.
(23) Gebauer, D.; Volkel, A.; Cölfen, H. *Science* **2008**, *322*, 1819–1822.

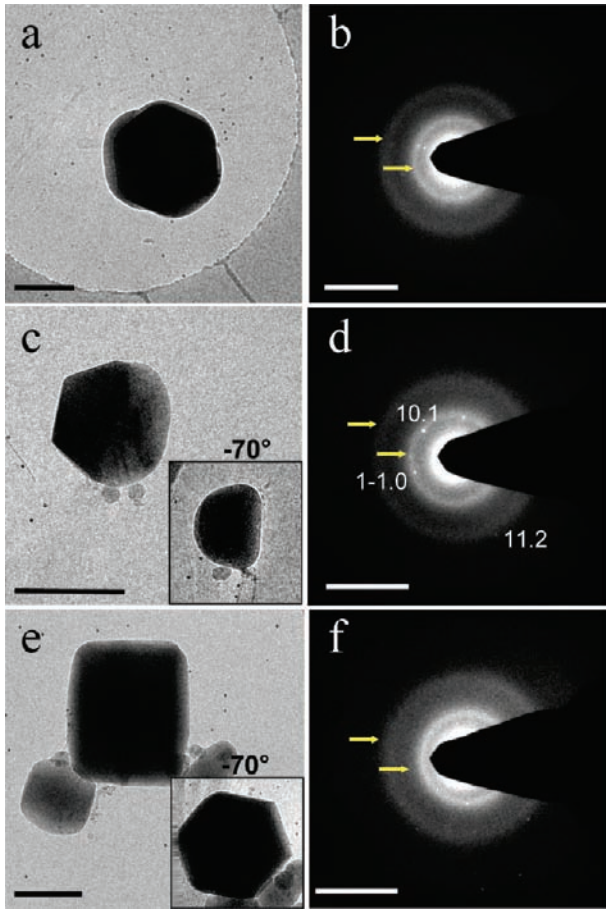

Figure 6. (a, c, and e) CryoTEM images of particles recorded after reaction times of 40 min. Insets: same particles recorded under a tilt angle of −70°. Scale bars = 400 nm. (b, d, and f) Corresponding LDSEAD of particles a, c, and e, respectively. The yellow arrows indicate the rings typical of the ACC. Scale bars = 5 nm^{-1}. Particle (a) is amorphous with polycrystalline domains, particle (c) shows a dominating pattern which corresponds to vaterite oriented [$\bar{1}$1.1], and particle (e) is also amorphous with polycrystalline domains despite the mature morphology.

clusters (Figure 8-**1**), as was recently reported by us[12] and others.[23,24] Similarly as was reported previously, these nanoparticles remain present in the solution throughout the entire reaction and should therefore represent the first stable form of solid calcium carbonate.[12] These small nanoparticles subsequently transform into a structurally probably more advanced population of ∼70 nm in size. Our observation of different sized ACC particles may be related to previous findings of ACC with different degrees of hydration,[9] different solubilities,[23] different stabilities under electron beam irradiation,[13] and different degrees of short-range order.[10] The bigger ones grow out to form particles with diameters >200 nm, a size that allows them to develop crystalline domains within the amorphous matrix. After nucleating, these domains first increase in number (Figure 5) and only later in size as judged by the highly polycrystalline nature of the particles (Figures 6 and 7) that precede the hexagonal crystals (Figures 2 and 8, **5**).

The above suggests that the development of the hexagonal single crystals occurs through the growth of domains that are stabilized by the interaction with NH_4^+ ions at the expense of the randomly oriented crystalline domains. As this process takes place within an amorphous matrix, it is most likely to occur

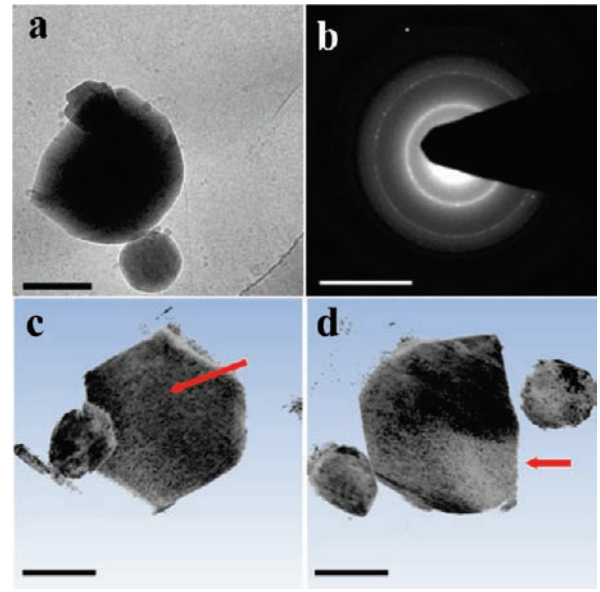

Figure 7. (a) CryoTEM image recorded after a reaction time of 30 min (scale bars = 200 nm) and (b) the corresponding LDSEAD (scale bar = 5 nm^{-1}). (c) Computer visualization of the cET of the particle (a) showing (red arrows) the stabilized (00.1) face of the vaterite crystals face on (c) and in profile (d). The movie of this 3D reconstruction is presented in Supporting Information 2.

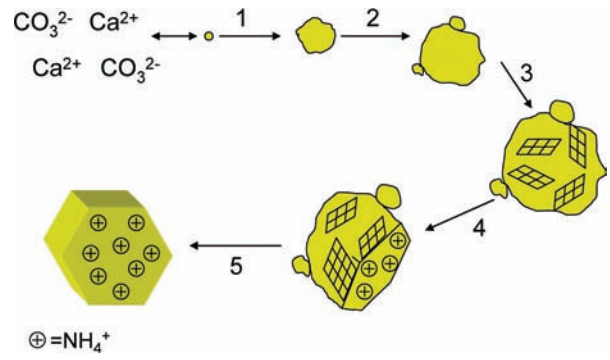

Figure 8. Scheme of the formation of the hexagonal platelets. Step 1: 35 nm ACC formed from the prenucleation clusters. Step 2: formation of a second population of ∼70 nm ACC particles. Step 3: development of the ACC into bigger particles allowing the development of randomly oriented crystalline domains (vaterite) coupled to the morphological development of the particle. Step 4: stabilization of the (00.1) face by the NH^{4+} ions. Step 5: inhibition of the growth in the (00.1) direction and formation of the hexagonal platelets.

via a solid state dissociation−recrystallization process (Figure 8, **4**). The development of crystallinity through a solid state transformation rather than through a dissolution−reprecipitation mechanism is further supported by the fact that the expression of the (00.1) face of vaterite precedes the development of the single crystalline character of the vaterite particles. The stabilized crystal face appears to act as a template from which crystallinity develops throughout the particle, in a similar manner as was described for monolayer directed crystal formation,[12] and in agreement with the model of Zhang et al.[19]

The development of multiple crystalline domains inside a single ACC particle suggests a solution-like character of the amorphous phase that allows separate nucleation events to take place. Moreover, the subsequent transformation into a single crystalline domain requires reorganization and therefore mass transport within the solid phase. It should be noted that the high

(24) Meldrum, F. C.; Sear, R. P. *Science* **2008**, *322*, 1802–1803.

degree of hydration in ACC may very well facilitate ion transport from one domain to the other. In particular, the presence of hydrated channels inside ACC, as recently proposed by Reeder et al., could be instrumental in this.[25]

In the colloidal 2D model system of Zhang et al., it was shown that initially created multiple metastable nuclei need to reach a critical size to become stable and to develop into a single crystal. In our system, this step is represented by the formation of multiple crystalline domains that are created inside the amorphous nanoparticles. Only when one of these nuclei reaches a critical size it will grow, and this will happen at the expense of the other metastable crystalline domains which are dynamically forming and dissociating. This results, just like in the model of Zhang and in our previous work, in only one mature crystal evolving from an amorphous particle.

Conclusion

In conclusion, we demonstrated that the formation of hexagonal plate-like vaterite occurs via an amorphous precursor phase. This amorphous phase converts into the crystalline state through a solid state transformation in which order and morphology develop simultaneously. The mineral initially develops as polycrystalline vaterite which transforms into a single crystal directed by an NH_4^+-induced crystal plane that acts as a templating surface. Moreover, these results demonstrate that the combination of cryoTEM, cET with diffraction and dark field imaging can reveal unprecedented details of biomimetic mineral formation.

Acknowledgment. This project was supported by The Netherlands Organization for Scientific Research (NWO). We thank J. van Roosmalen for his help with the visualization of the tomograms.

Supporting Information Available: Detailed experimental section (PDF file) and movies (mpg files) of the tilt-series and 3D reconstructions of the particles shown in Figures 5 and 7. This material is available free of charge via the Internet at http://pubs.acs.org.

JA102439R

(25) Goodwin, A. L.; Michel, F. M.; Phillips, B. L.; Keen, D. A.; Dove, M. T.; Reeder, R. J. *Chem. Mater.* **2010**, *22*, 3197–3205.